M. Ayub, A. C. Zander, D. M. Huang, C. Q. Howard and B. S. Cazzolato
Molecular dynamics simulations of acoustic absorption by a carbon nanotube
Physics of Fluids, 2018; 30(6):066101-1-066101-15

Molecular dynamics simulations of acoustic absorption by a carbon nanotube

M. Ayub,[1,a)] A. C. Zander,[1] D. M. Huang,[2] C. Q. Howard,[1] and B. S. Cazzolato[1]
[1]*School of Mechanical Engineering, The University of Adelaide, Adelaide, SA 5005, Australia*
[2]*Department of Chemistry, School of Physical Sciences, The University of Adelaide, Adelaide, SA 5005, Australia*

(Received 21 February 2018; accepted 21 May 2018; published online 7 June 2018)

Acoustic absorption by a carbon nanotube (CNT) was studied using molecular dynamics (MD) simulations in a molecular domain containing a monatomic gas driven by a time-varying periodic force to simulate acoustic wave propagation. Attenuation of the sound wave and the characteristics of the sound field due to interactions with the CNT were studied by evaluating the behavior of various acoustic parameters and comparing the behavior with that of the domain without the CNT present. A standing wave model was developed for the CNT-containing system to predict sound attenuation by the CNT and the results were verified against estimates of attenuation using the thermodynamic concept of exergy. This study demonstrates acoustic absorption effects of a CNT in a thermostatted MD simulation, quantifies the acoustic losses induced by the CNT, and illustrates their effects on the CNT. Overall, a platform was developed for MD simulations that can model acoustic damping induced by nanostructured materials such as CNTs, which can be used for further understanding of nanoscale acoustic loss mechanisms associated with molecular interactions between acoustic waves and nanomaterials. *Published by AIP Publishing.* https://doi.org/10.1063/1.5026528

I. INTRODUCTION

Interest in carbon nanotubes (CNTs) for various applications has grown rapidly because of their extraordinary properties and versatility in forming composite nanostructures. In particular, structures can be fabricated with modified mechanical and thermal properties that act as promising sound-absorption materials for noise control.[1–3] In addition, the emergence of advanced manufacturing technologies offers exciting possibilities for creating tailored acoustic absorbers using CNTs.[2–4] The potential of CNTs and composite absorbers for use in noise-control applications has been investigated in various studies.[5–9] Moreover, the acoustic absorption properties of CNTs have been measured in several studies.[10–12] These investigations have yielded promising results for the absorption characteristics of CNTs and highlighted the need for improved understanding of the absorption mechanisms of nanoscopic fibers at the nanoscale.[13–15]

The mechanisms of sound absorption for conventional porous acoustic materials with fiber diameters or pores on the micro-scale (down to 1 μm) are currently well understood. The relative influence of the various mechanisms is, however, expected to change for materials with pores or fibers at the smaller nanoscale (down to 1 nm), while other mechanisms and nonlinear effects may also become significant. Theoretical and computational approaches such as molecular simulations can play an important role in shedding light on the detailed mechanisms by which nanomaterials absorb sound. However, conventional molecular dynamics (MD) simulations assume some conserved quantity, and thus it is not straightforward to measure the dissipation of acoustic energy. Thus, a method to quantify the attenuation of acoustic energy during sound wave propagation in a medium (gas) interacting with a nanomaterial is needed in order to model sound absorption in a thermostatted molecular dynamics simulation.

The classical sources of attenuation in a sound wave are internal viscous friction and heat conduction. However, if the wave-propagation domain contains a solid material along with a gas, additional losses may occur due to the interactions between the two media. The interactions trigger an energy exchange between the fluid and the solid in the vicinity of the solid surface and creates a region, known as the viscous boundary layer, where the mean flow velocity varies from zero at the surface to the free stream velocity far from the surface. The presence of this region causes a viscous loss of the sound energy as viscous stresses oppose the fluid motion and dissipate the fluid kinetic energy as heat.[16] In addition, thermal losses can occur due to heat conduction to the solid surface within the thermal boundary layer, which results from the temperature gradient created by the transition of the wave-propagating media from the isothermal condition at the solid surface to the isentropic (adiabatic) condition far from the surface.[17] In conventional computer simulations of acoustic wave propagation (such as computational fluid dynamics), acoustic losses (thermal and viscous) are defined using continuum theory and the losses are quantified as a function of sound attenuation based on continuum fluid assumptions.[18,19] However, the theoretical approximations of attenuation for an acoustic system based on a fluid continuum are only applicable at low frequencies, where the relaxation time for absorption (viscous and thermal) is similar to the mean time between collisions.[13,20] Hence, the estimates of acoustic losses based on the theory of continuum mechanics may not be applicable to acoustic wave

a)Electronic mail: md.ayub@adelaide.edu.au

propagation in a gas at the nanoscale. Hadjiconstantinou and Garcia[21] conducted direct simulation Monte Carlo (DSMC) simulations of sound wave propagation in the gigahertz (GHz) range without any solid present in the simulation domain. They calculated the sound speed and attenuation coefficient by non-linearly fitting the simulated velocity amplitude, assuming plane-wave theory. The results were found to be significantly affected by free molecular flow near the sound source during a high-frequency sound wave propagation, for which the wavelength was comparable to the mean free path. Thus, the calculated sound speed and attenuation coefficient were sensitive to the distance from the sound source used for curve fits.[21] Therefore, a method that can accurately measure acoustic losses in a molecular system without relying on factors such as free molecular flow or continuum approximations is highly desirable. Here, a simulation framework for molecular dynamics was developed to study the sound field characteristics of high-frequency wave propagation in a simple monatomic gas in a simulation domain containing a CNT with the aim of investigating the acoustic losses due to the CNT and to capture the atomistic mechanisms involved. Losses occur both due to the conversion of the coherent acoustic energy into random thermal energy as the wave propagates and due to the atomistic interactions between the acoustic wave and the CNT. A notable contribution of this work is to identify the acoustic damping in the MD simulations and to quantify the acoustic absorption of the CNT using the thermoacoustic concept of exergy,[22] in which the dissipation of acoustic energy (acoustic losses) is defined in terms of entropy generation. Exergy is a thermodynamic potential that measures the ability to do useful work in a system in the presence of a freely accessible thermal reservoir at a particular temperature.[22] Acoustic losses evaluated using this method are compared with the estimates from standing-wave theory[15,21] developed for a system of acoustic wave propagation containing both the gas and the CNT. Additional MD simulations were also performed for sound wave propagation in a domain without the CNT present to distinguish the losses in the CNT-containing system from the classical acoustic losses in the fluid medium. The framework for MD simulations and the analysis of the sound field demonstrated in this study can be extended to investigate the loss mechanisms in systems containing more CNTs or other nanomaterials. It should also be noted that the MD simulation framework (without the CNT present) used here was validated by the authors in a previous publication[15,23] comparing Hadjiconstantinou and Garcia's[21] results from DSMC simulations and with the theoretical estimate of the transmission matrix method[24] of a duct system, which showed comparable particle velocity amplitudes in the simulation domain.

This paper is organized as follows. Details of the simulated system and simulation protocol are described in Sec. II. Section III presents the relevant theories and calculation methods used to estimate the acoustic losses and attenuation coefficient. The simulation results for the acoustic behavior and acoustic losses in systems with and without a CNT are compared in Sec. IV. The effects of interactions with the acoustic wave on the CNT are explained in Sec. V.

II. SIMULATION DETAILS

For simplicity, this work considers acoustic absorption effects of a CNT arising only from interactions between the acoustic wave and the outer surface of the CNT. Figure 1 shows a schematic of a system of nanotubes vertically aligned with respect to the substrate to represent a CNT forest with millions of nanotubes per square centimeter grown on a silicon substrate, in which interaction of sound waves occurring with and between the tubes. To understand the interaction of multiple tubes with acoustic waves, it is first necessary to determine the sound wave propagation behavior around a single tube, as the sound absorption by each tube is also expected to contribute significantly to the total absorption. Moreover, due to the limited availability of computational resources, simulations were restricted to a relatively short and narrow CNT. In the work presented in this study, the analysis of a single CNT fibre in a small acoustic domain was considered, where typical solution times were on the order of 25 days (per 100 periods of the wave cycle) using 96 CPU cores of a supercomputer.

MD simulations were performed for a plane sound-wave propagation in a monatomic argon gas in a rectangular domain at a frequency of $f \approx 1.5$ GHz. The simulating domain is illustrated in Fig. 1. An oscillating wall comprising a closed-packed FCC (face-centered cubic) lattice of "solid" argon atoms was used as the sound source and excited at $z = 0$ with a velocity assigned to wall atoms collectively by imposing a sinusoidally varying velocity in the z-direction. The piston wall was constructed by holding a collection of 35 645 argon atoms fixed with respect to one another in an FCC lattice with one face of the atoms exposed to the gas. The wall of solid argon, combined

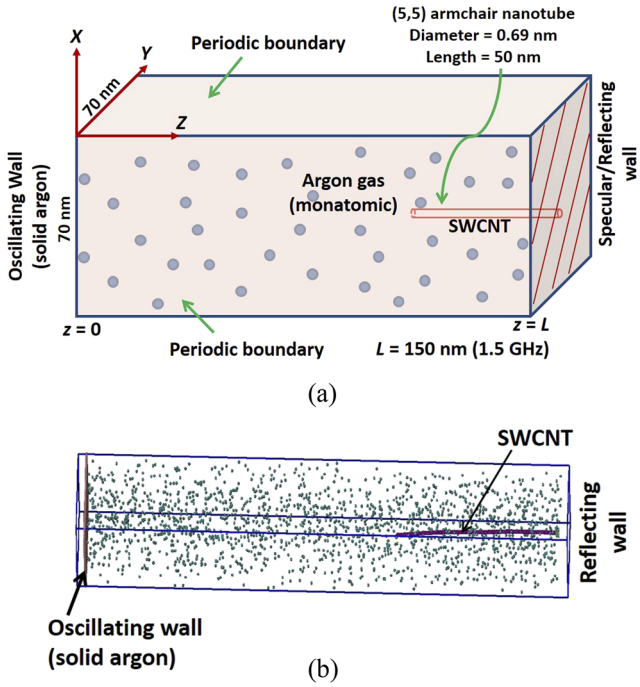

FIG. 1. Simulation domain and sound source model for acoustic wave propagation in argon gas with the immersed CNT. The schematic is not drawn to scale. (a) Schematic of simulation geometry. (b) Snapshot of the MD simulation domain.

with the thermostat applied to the gas, was designed to mimic a diffuse reflection boundary condition. During the simulation, the piston was oscillated back and forth with a sinusoidally varying velocity in the direction perpendicular to its surface, while the thermostat imposed a Maxwell-Boltzmann distribution at the desired temperature on the velocity components of the gas atoms perpendicular to the wave propagation direction. The far end of the simulation domain in the z-direction was terminated by a specular reflecting wall, and the system was replicated in the transverse directions using periodic boundary conditions. The domain was filled with argon gas at a density of $\rho = 1.8$ kg m^{-3} (20 402 molecules) to maintain the average gas pressure at $P = 1$ atm.

An open-end (uncapped) (5, 5) single-walled carbon nanotube (SWCNT) of length $L_{\mathrm{CNT}} = 50$ nm and diameter $d_{\mathrm{CNT}} = 0.69$ nm was cantilevered at the specular wall and immersed in the simulation domain. One end of the CNT, consisting of atoms within 0.1 nm of the clamped boundary, was fixed and the remainders of the CNT atoms were allowed to move freely according to the interaction forces on them. The small size (diameter and length) of the CNT was chosen in order to reduce the computational expense and to simplify the atomistic mechanisms by ensuring that gas atoms could not enter the interior of the CNT. The simulation domain had dimensions of $L_z = 150$ nm in the wave-propagation direction and $L_x = L_y = 70$ nm transverse to the wave-propagation direction. The domain size was large enough to exclude inter-nanotube coupling interactions between periodic images. With the periodic boundary conditions applied in the directions perpendicular to the propagation direction, the simulated system represents an array of nanotubes with an area density of 0.0002 nm^{-2} and an intertube spacing of 70 nm, which is similar to an experimental CNT array investigated in the authors' previous work.[10,12] The evenly spaced CNT alignment would thus represent a simple cubic array (or a planar repeating pattern) of nanotubes. Although this arrangement of nanotubes is an approximation, it is a reasonably realistic representation of the types of nanotube arrays that can be achieved experimentally by growing patterned CNTs on a surface.[2,3]

It should also be noted that the potential of resonant interactions between nanotubes is small given that all simulations were performed with larger dimensions of 70 nm to ensure that the domain size was at least of similar size to one mean free path (≈72 nm) of the gaseous argon atoms. Having a large enough system size to accommodate a full collision length for gaseous atoms would minimise/exclude inter-nanotube coupling interactions via the gaseous argon atoms as a result of the periodic boundary condition in the lateral directions. In addition, the effect of changing the periodicity of the simulation box in the lateral directions was checked by performing simulations for varying domain lengths in the lateral directions of 20 nm to 70 nm with the domain length in the wave-propagation direction fixed at 150 nm. These simulations showed that the results for all measured quantities converged for lateral dimensions larger than 60 nm (equivalent to $\frac{L_x \text{ or } L_y}{\lambda_{\mathrm{mfp}}} \gtrsim 1$, where L_x and L_y are domain lengths in the lateral directions and λ_{mfp} is the mean free path of the gas).

A second generation REBO (reactive empirical bond order)[25] potential was used to model the inter-atomic interactions between carbon atoms in the CNT. The REBO potential has been used widely by researchers[26] to perform MD simulations of carbon nanotubes. It has been successfully used to calculate the thermal transport properties of carbon nanomaterials.[26] In addition, it is known for its accuracy to reproduce the phonon dispersion relations of CNTs, which is very important for heat transfer mechanisms.[26–29] The interactions between argon gas molecules were described by a Lennard-Jones (LJ) 12-6 potential with LJ parameters $\varepsilon_{AA} = 10.33$ meV and $\sigma_{AA} = 3.40$ Å and a cut-off distance of $3\sigma_{AA}$.[26] The inter-atomic interactions between argon and carbon atoms (argon-carbon) were also represented by a LJ potential with parameters $\varepsilon_{\mathrm{AC}} = 4.98$ meV and $\sigma_{\mathrm{AC}} = 3.38$ Å.[26] A short-range purely repulsive WCA (Weeks-Chandler-Andersen) potential[30] with the same LJ parameters was used for the interaction between the atoms of the solid wall and those of the propagating medium (gas) by truncating the LJ potential at $2^{\frac{1}{6}}\sigma_{ij}$. These parameters were chosen based on their applications in similar studies of the phenomena relevant to acoustic modeling of carbon nanotubes such as fluid/structure interactions, bi-directional heat transfer, and acoustic wave propagation.[15,26–29,31] The total number of atoms in the simulation domain, $N_{\mathrm{system}} = 60\,127$ (with $N_{\mathrm{wall}} = 35\,645$, $N_{\mathrm{argon\ gas}} = 20\,402$, $N_{\mathrm{CNT}}^{\mathrm{free}} = 3990$, and $N_{\mathrm{CNT}}^{\mathrm{fixed\ end}} = 90$), was constant during the simulations.

Simulations were initiated with a small time step of 0.01 fs using a velocity-Verlet algorithm in order to relax the system; the time step was gradually increased to 0.4 fs. Thereafter, simulations were continued with a time step of 0.5 fs. The initial velocities of the gas molecules were chosen randomly from a Gaussian distribution consistent with a temperature of 273 K, while the CNT atoms were initially stationary (i.e., at a temperature of 0 K). The gas molecules and CNT were coupled to two separate Langevin thermostats, both at 273 K during an equilibration period of 15 ns. After the equilibration, the system was excited by an acoustic wave generated by oscillating the solid wall with a velocity amplitude of $v_0 = 0.15c = 49.69$ ms^{-1} (where c is the classical sound speed) and frequency of 1.5 GHz ($R = 1$, where R is the acoustic Reynolds number[21]). During the simulation of high-frequency sound-wave propagation, an auxiliary mechanism was required to remove the added heat resulting from the work done on the system by the rapid oscillation of the sound source. Hence, a Nosé-Hoover thermostat at $T = 273$ K was coupled loosely [with a thermostatting damping time (τ) of 1 wave period] to the degrees of freedom of the gas molecules perpendicular (x and y) to the propagating wave (z-direction) to control the temperature. This thermostat mimics the interaction of the gas with a thermal reservoir surrounding the simulated system in the directions perpendicular to the wave-propagation direction, as would be the case in a real physical system. The CNT was not directly thermostatted during the acoustic wave propagation. As the flow reached the steady state, sampling was carried out for a total duration of 40 wave-cycle time periods.

III. CNT-INDUCED ATTENUATION: CALCULATION METHODS

Sound attenuation due to the interaction between the sound wave and the CNT was evaluated using both curve fitting based on standing wave theory and the thermodynamic concept of exergy. The development of the equations and the calculation methods are described in Secs. III A and III B.

A. Standing-wave theory

Curve fitting of the waveform components over an entire domain (as discussed in previous studies[15,21]) is not appropriate in the current study because there are two coupled domains: one between the source and the tip of the CNT, which contains only argon atoms, and another for the remainder of the domain, which contains both argon and CNT atoms. Hence, standing-wave equations based on classical acoustic wave theory were formulated for an acoustic domain incorporating a CNT by considering two separate domains between the source and receiver, as illustrated in Fig. 2.

The rectangular simulation domain of cross-sectional area $S = (L_x \times L_y)$ and length L_z was subdivided into two separate regions of length $L' < z < L$ (*Region* 1) and $0 < z < L'$ (*Region* 2), respectively, with the boundary between the two regions at $z = L'$. Wave propagation was driven by a piston at $z = 0$. The domain was terminated by a reflecting wall at $z = L$. If the piston oscillates harmonically at a frequency ω, then the superposition of the incident and reflected waves on each side leads to a standing wave which can be expressed in a generalized form of wave equation as

$$v_{g/c}(z,t) = A_{g/c}(z)\ \sin\omega t + B_{g/c}(z)\ \cos\omega t. \tag{1}$$

Here, $A_{g/c}(z)$ and $B_{g/c}(z)$ are the components of the velocity amplitude of the standing wave on each side, where for the CNT region (*Region* 1),

$$A_c(z) = v_0\ [e^{-m_c z}\ \cos kz\ -\ e^{m_c(z-2L)}\ \cos k(z-2L)], \tag{2}$$

$$B_c(z) = -v_0\ [e^{-m_c z}\ \sin kz\ +\ e^{m_c(z-2L)}\ \sin k(z-2L)], \tag{3}$$

and for the gas region (*Region* 2),

$$A_g(z) = v_0\ [e^{-m_g z}\ \cos kz\ -\ e^{m_g z-2m_c L}\ \cos k(z-2L)], \tag{4}$$

$$B_g(z) = -v_0\ [e^{-m_g z}\ \sin kz + e^{m_g z-2m_c L}\ \sin k(z-2L)], \tag{5}$$

where $k = \omega/c$ is the acoustic wave number, ω is the angular frequency, c is the classical sound speed, and m is the attenuation constant. The derivation of these equations is described in Appendix A. Equations (2)–(5) also can be rearranged to form the standing wave equation for a single region between the source and receiver which contains only gas atoms similar to the case discussed in the DSMC study by Hadjiconstantinou and Garcia.[21] By replacing $m_g = m_c = m$ for the case without CNT, one may obtain the equations of velocity components as

$$A(z) = v_0\ [e^{-mz}\ \cos kz\ -\ e^{-m(2L-z)}\ \cos k(2L-z)], \tag{6}$$

$$B(z) = -v_0\ [e^{-mz}\ \sin kz\ -\ e^{-m(2L-z)}\ \sin k(2L-z)], \tag{7}$$

which represent velocity components of a standing wave for a single region of gas atoms between the source and receiver. Verification of the standing wave profile of two-region approach against that of a single region between the source and receiver are also discussed in Appendix A.

Furthermore, it should be noted that the attenuation coefficient m_c represents sound attenuation in the CNT region, which has both gas and a CNT, hence the resultant attenuation by the CNT would only be $(m_c - m_g)$. If the CNT induces any acoustic absorption in the gas, then m_c has to be larger than m_g. The acoustic absorption coefficient within the CNT region can be estimated from the calculated attenuation constant (m_c) using the relationship between the reflection coefficient (R_α) and attenuation constant as[32]

$$R_\alpha = \exp[-(ik + m_c)\,2L_1]. \tag{8}$$

Similarly, the reflection coefficient for CNT only can be expressed as

$$R_\alpha^{\mathrm{CNT}} = \exp[-(ik + m_c - m_g)\,2L_{\mathrm{CNT}}]. \tag{9}$$

The resultant absorption coefficient is then calculated as[19]

$$\alpha = 1 - \left|R_\alpha^{\mathrm{CNT}}\right|^2. \tag{10}$$

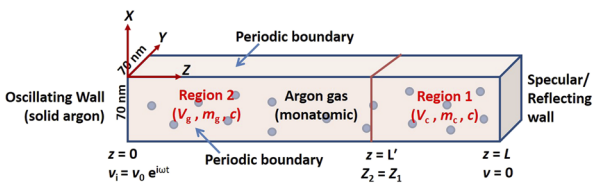

FIG. 2. Schematic of the subdivision of the simulation domain into two separate regions for the standing-wave theory analyses: one between the source and tip of the CNT containing only argon atoms (*Region* 2) and another for the remainder of the domain containing both argon and the CNT (*Region* 1). Variables for the particle velocity and attenuation constant in each region are represented by (v_g, m_g) for *Region* 2 and by (v_c, m_c) for *Region* 1. The sound speed (c) was assumed to be the same in both regions.

B. Exergy analysis

The acoustic energy losses in the system can also be evaluated using exergy, a thermoacoustic potential that measures the ability to do useful work in a system in the presence of a freely accessible thermal reservoir at a particular temperature T_0. A detailed description of exergy can be found in the book by Swift,[22] in which the losses of acoustic energy in a system are considered as lost work $(\dot{W}_{\mathrm{lost}})$ and estimated as entropy generation, which is responsible for the irreversibility of processes in the system. A similar approach of energy balance has been applied here. A schematic of a generalized microscopic portion of an acoustic system in the presence of a CNT is shown in Fig. 3. Following the method described by Swift,[22] the entropy generation in this domain can be expressed as

$$T_0 \sum \dot{S}_{\mathrm{gen}} = \dot{W}_{\mathrm{lost}} = \dot{X}_{\mathrm{In}} - \dot{X}_{\mathrm{Out}}, \tag{11}$$

where $\dot{X}(z)$ is the time-averaged exergy flux in the z-direction (the subscripts "In" and "Out" denote fluxes into and out of the domain, respectively), which can be written as

$$\dot{X} = \frac{T_0}{T_m}\dot{E} + \left(1 - \frac{T_0}{T_m}\right)\dot{H}, \tag{12}$$

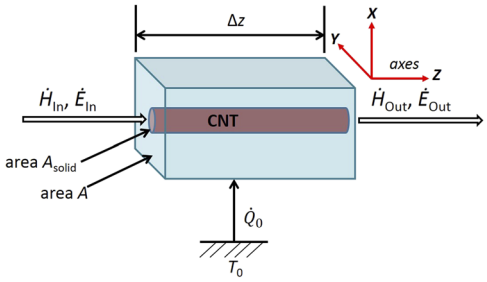

FIG. 3. Schematic of the generalized microscopic portion of the simulation domain containing a CNT. The wave propagates in the z-direction. This portion of the simulation domain with length Δz has acoustic power $\dot{E}_{\mathrm{In(Out)}}$ and total power $\dot{H}_{\mathrm{In(Out)}}$ flowing into the left side (out of the right side). The system rejects (or absorbs) thermal power $\dot{Q}_0$ to ambient at T_0. The schematic is adapted from Ref. 22.

where $\dot{E}$ is the acoustic power flowing at a mean temperature T_{m} along the wave path, which is equal to active acoustic intensity I_{ac} when presented as an acoustic power flowing per unit area in a plane-wave propagation. The active acoustic intensity I_{ac} can be associated with the particle velocity, $v(z,f)$, and sound pressure, $p(z,f)$, of the standing wave as[19,33,34]

$$I_{\mathrm{ac}} = \frac{1}{2}\mathrm{Re}[pv^*]. \tag{13}$$

Here, v^* is the complex conjugate of the particle velocity $v(z,f)$.

The total power flux, $\dot{H}(z)$, in the z-direction is[35]

$$\dot{H}(z) = \frac{1}{2}\rho \int Re[hv^*]dA - (A\kappa + A_{\mathrm{solid}}\kappa_{\mathrm{solid}})\frac{\mathrm{d}T_{\mathrm{m}}}{\mathrm{d}z}, \tag{14}$$

where h ($=U + PV = E_{\mathrm{k}} + E_{\mathrm{p}} + P/\rho$) is the enthalpy per unit mass, κ is the thermal conductivity, A is the cross-sectional area, T_{m} is the mean temperature of the gas, and the subscript "solid" denotes properties of whatever solid is present in the system. The first term on the right side of Eq. (14) is the time-averaged enthalpy flux and the second term is the conduction of heat both in the gas and in the solid present in the system. Here, U is the sum of the total kinetic (E_{k}) and potential (E_{p}) energies, P is the pressure, and V is the volume of the gas.

Equation (12) for the exergy flux $\dot{X}$ denotes the associated power to do work in the presence of a thermal reservoir at T_0.[22] Dividing the full simulation domain into M "bins" in the wave-propagation direction and expressing $\dot{X}_{\mathrm{In}} = \dot{X}^i$ and $\dot{X}_{\mathrm{Out}} = \dot{X}^{i+1}$, where i(=1, 2, 3, . . ., M) is the bin number index, Eq. (11) can be expressed as

$$T_0\frac{\mathrm{d}\sum \dot{S}_{\mathrm{gen}}}{\mathrm{d}z} = \lim_{\Delta z\to 0} -\frac{\dot{X}^{i+1} - \dot{X}^i}{\Delta z} = -\frac{\mathrm{d}\dot{X}}{\mathrm{d}z}. \tag{15}$$

The entropy generation calculated using Eq. (15) gives the rate of energy lost per unit length of the microscopic portion of the thermoacoustic system. For a simulation domain of a thermoacoustic system of plane-wave propagation of volume V, cross-sectional area A, and length L_z containing a CNT of length $L_{\mathrm{CNT}} = L_z$ and cross-sectional area A_{CNT}, the rate at which the energy per unit volume is lost from the wave is

$$\frac{\dot{W}_{\mathrm{lost}}}{V} = -\frac{1}{V}\left[\int_0^{L_z} \nabla\dot{X}dz\right]. \tag{16}$$

In the current simulation, the CNT was placed at the termination wall and the length of the tube L_{CNT} was smaller than the total length of the simulation domain L_z. Hence heat conduction between the gas and the CNT can be considered to be limited to a region of length L_{CNT}. Therefore the simulation domain can be subdivided, similar to the schematic in Fig. 2, into two adjacent regions: one containing only gas atoms in which heat conduction occurs only in the gas and another containing both gas atoms and the CNT in which the conduction of heat occurs both in the gas and in the CNT. This can be realized by separating the heat conduction terms in the calculation of the total power flux using Eq. (14). The total power flux can be expressed as

$$\dot{H}(z) = \dot{H}_{\mathrm{g}} - \dot{h}_{\mathrm{CNT}}, \tag{17}$$

where $\dot{H}_{\mathrm{g}}$ is the total power flux without the heat conduction term for the CNT and $\dot{h}_{\mathrm{CNT}}$ is the heat conduction term for the CNT. These terms can be written as

$$\dot{H}_{\mathrm{g}}(z) = \frac{1}{2}\rho \int Re[hv^*]dA - A\kappa\frac{\mathrm{d}T_{\mathrm{m}}}{\mathrm{d}z}, \tag{18}$$

$$\dot{h}_{\mathrm{CNT}}(z) = A_{\mathrm{CNT}}\kappa_{\mathrm{CNT}}\frac{\mathrm{d}T_{\mathrm{m}}}{\mathrm{d}z}. \tag{19}$$

Combining Eqs. (17)–(19), the thermoacoustic approximation for the exergy flux $\dot{X}$ in Eq. (12) can be rearranged for the gas in the absence of any solid in the system as

$$\dot{X} = \frac{T_0}{T_{\mathrm{m}}}\dot{E} + \left(1 - \frac{T_0}{T_{\mathrm{m}}}\right)\dot{H}_{\mathrm{g}}. \tag{20}$$

Substitution into Eq. (16) gives a generalized equation for the entropy generation (lost work) in a simulation domain containing a CNT,

$$\frac{\dot{W}_{\mathrm{lost}}}{V} = -\frac{1}{V}\int_0^{L_z} \nabla\dot{X}\mathrm{d}z + \frac{1}{V}\left(1 - \frac{T_0}{T_{\mathrm{m}}}\right)\int_{L_z - L_{\mathrm{CNT}}}^{L_z} \nabla\dot{h}_{\mathrm{CNT}}\mathrm{d}z, \tag{21}$$

where $(L_z - L_{\mathrm{CNT}})$ is the length of the domain containing gas atoms only, which represents a domain similar to *Region* 2 in Fig. 2. Equation (21) gives the power lost per unit volume, which can then be used to obtain the attenuation coefficient $m_{\mathrm{e}}^{\mathrm{cnt}}$ as

$$m_{\mathrm{e}}^{\mathrm{cnt}} = -\frac{\left[\frac{\dot{W}_{\mathrm{lost}}}{V}\right]}{2I}, \tag{22}$$

where $I(=\frac{1}{2}\rho c v_0^2)$ is the classical acoustic intensity for the simulated wave, $v_0 = 49.69\ \mathrm{ms}^{-1}$ is the particle velocity amplitude chosen for the study, and the subscript "e" is used to indicate an estimate based on the exergy.

IV. SIMULATION RESULTS AND DISCUSSIONS

Following equilibration, the simulations were run for 67.35 ns, which is equivalent to 100 periods of the propagating wave cycle, which was at a frequency of $f \approx 1.5$ GHz. The energy balance of the system and the variation of the temperature of both the gas and the CNT and of the gas pressure during the wave propagation were monitored to observe the state of the flow and to check the effect on the sound speed due to dissipation. Details of these parameters can be found in Appendix B.

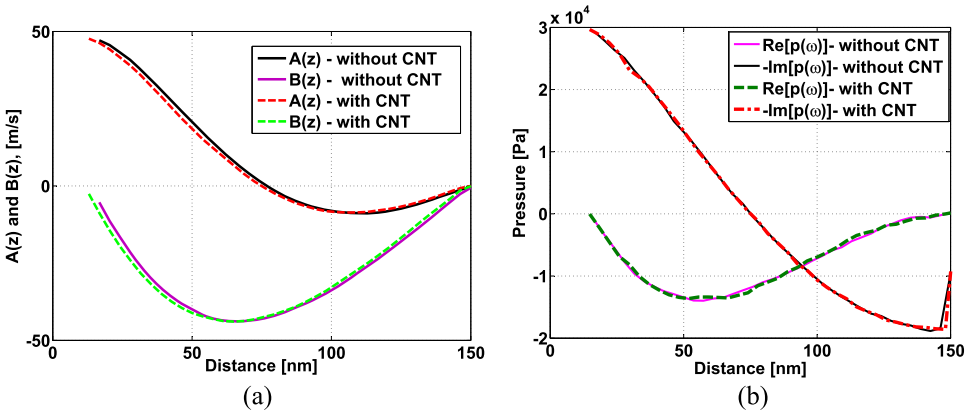

FIG. 4. (a) Components, $A(z)$ and $B(z)$, of particle velocity amplitude $v(z)$ and (b) real and imaginary components of the acoustic pressure $p(z)$ of the acoustic wave at a frequency of $f \approx 1.5$ GHz in a simulation with and without a CNT present for the same simulation conditions.

A. Sound field

To observe the effect of the interaction between the CNT and the gas on acoustic parameters such as the velocity profile, acoustic active and reactive intensity, and absorption coefficient, the acoustic sound field behavior was compared between the cases with and without the CNT for the same simulation conditions. Figure 4 shows comparisons of the velocity components, $A(z)$ and $B(z)$, of the particle velocity amplitudes $v(z)$ and the real and imaginary components of acoustic pressure $p(z)$ as a function of distance for both cases. It can be observed that the velocity and pressure components do not reveal any substantial differences between the two cases. Similarly no considerable differences are observed in the active and reactive intensities[33] of the sound field shown in Fig. 5.

The reason for these insubstantial differences in the acoustic components between the simulations with and without the CNT can be attributed to the small differences between the attenuation coefficients for the regions of the gas only (*Region* 2) and the gas with CNT (*Region* 1). So to observe any considerable changes in the acoustic variable profiles, the attenuation coefficient in the CNT region must be significant compared with that in the gas region. However, as demonstrated below, an analysis of the power balance in the system in terms of exergy reveals considerable differences between the simulations with and without the CNT.

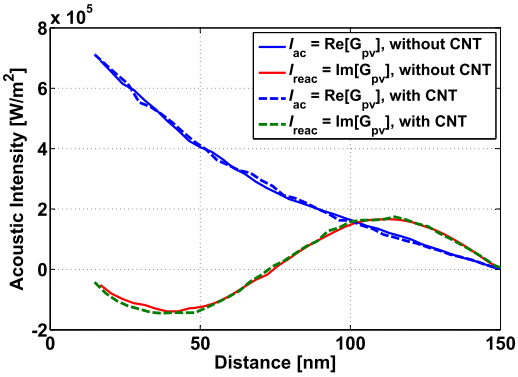

FIG. 5. Active and reactive acoustic intensities, I_{ac} and I_{reac}, as a function of distance in a simulation with and without a CNT present for the same simulation conditions. Here, G_{pv} is the cross power spectrum between the sound pressure and particle velocity.

A similar comparison of the transfer function, $H_{p_0p_z}$, between the acoustic pressure at the sound source (p_0) and that away from the source (p_z), for the simulations with and without the CNT is displayed in Fig. 6. The local acoustic absorption coefficient as a function of distance along the wave path is also compared for the two simulations and presented in Fig. 7. Again, no considerable changes in the absorption coefficient are observed even near to the tip of the CNT ($z \approx 99.9$ nm) or within the distance from the tip of the CNT to the termination wall.

However, it can also be seen that the components of the acoustic intensities and transfer function between acoustic pressures at the source and away from the source, as shown in Figs. 5 and 6, in the presence of CNT show small but discernible changes in the corresponding profiles compared with those in the simulation without the CNT, which can be attributed to the interaction between the acoustic wave and the CNT and the subsequent changes to the acoustic energy in the system. These indicate the introduction of attenuation due to the presence of the CNT and its interaction with the wave, much like what would be expected as a result of increasing noise (due to attenuation) in the signal as a function of frequency for high-frequency wave propagation. These responses also show that some of the energy in the system must have gone into the structure, which therefore alters the resulting pressure response and ensures effective re-distribution of total energy into two systems of gas and CNT; hence, the discernible changes in pressure dependent quantities once the CNT is included.

B. Sound attenuation

From Sec. IV A, it can be seen that the components of the velocity amplitude in the presence of the CNT show a small but discernible change compared with those in the simulation without the CNT. Non-linear curve fitting, using the two-region approach described in Sec. III A, to the velocity components $A(z)$ and $B(z)$ of the acoustic domain containing a CNT gives a value of 1.21×10^7 m^{-1} for the attenuation coefficient m_c for the CNT region (*Region* 1) by assuming a constant value of $m_g = 1.05 \times 10^7$ m^{-1} and a sound speed of $c = 431$ ms^{-1} for the gas obtained from fitting the velocity profile within $z > 100$ nm equal to *Region* 1 in the simulation without the CNT. The fitting of the simulation results is

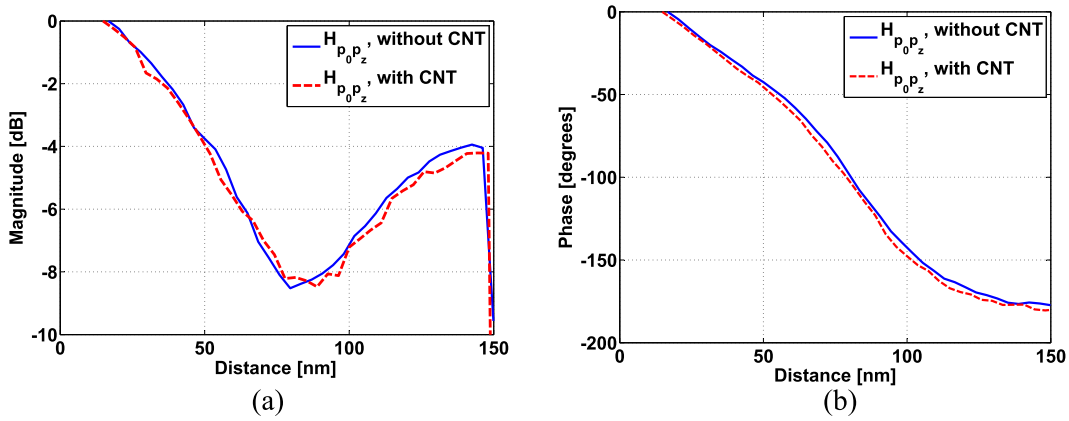

FIG. 6. (a) Magnitude (dB) and (b) phase (degree) of the transfer function, $H_{p_0p_z}$, between the acoustic pressure at the sound source and that away from the source, as a function of distance in a simulation with and without a CNT present for the same simulation conditions.

illustrated in Fig. 8. The value of $m_c > m_g$ indicates the occurrence of additional absorption of acoustic energy by the CNT in the CNT region. Hence, the value of $(m_c - m_g)$ represents the attenuation by the CNT only.

These findings can be verified by estimating the attenuation coefficients using a more rigorous approach for the energy balance provided by the exergy, as described in Sec. III B. Estimates of the acoustic power $\dot{E}$, total power $\dot{H}$, and exergy $\dot{X}$ for the simulation containing the CNT are shown in Fig. 9. The largest differences between the exergy and acoustic power can be observed in the CNT region of the domain along the wave path of $z > 90$ nm, indicating additional consumption of acoustic energy by the CNT compared with the CNT-free region. These differences are more pronounced when these curves are compared with that of the simulation containing gas only, as shown in Fig. 10. These results illustrate the considerable utility of exergy for analyzing nanoscale acoustic absorption. In the preceding estimates of acoustic parameters, only a subtle difference between the acoustic power curves (Fig. 5) was observed between the simulations with and without the CNT, which were calculated based on the changes in the acoustic pressure and particle velocity. However, unlike the velocity components or acoustic power, substantial differences in the exergy and total power curves can be seen in Fig. 10 in the two simulations, particularly in the region containing the CNT, whereas no substantial changes occur in the gas region $z < 90$ nm. From the exergy, the attenuation coefficient (m_e^{cnt}) for the whole system with the CNT present was calculated using Eq. (21). The value of $m_e^{cnt} = 2.17 \times 10^7$ m^{-1} calculated form the exergy is approximately equal to the value of $(m_c + m_g) = 2.26 \times 10^7$ m^{-1} obtained from curve fitting using the two-region approach. Note that the value of m_c represents only the CNT region; hence, the value of $(m_c + m_g)$ represents the attenuation for the whole system combining both the gas and CNT regions in Fig. 2. The discrepancy can be attributed to the curve fitting methods of one-region and two-region approaches of the standing wave equation used for obtaining attenuation coefficient m_g for gas atoms only.

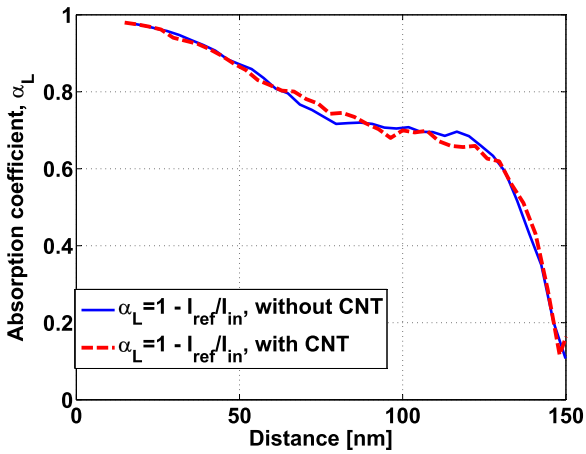

FIG. 7. Local acoustic absorption coefficient, α_L, as a function of distance along the wave path in a simulation with and without a CNT present for the same simulation conditions.

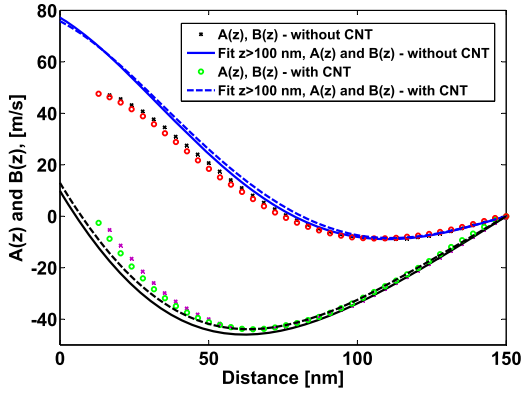

FIG. 8. Curve fit, using the two-region approach described in Sec. III A, to cosine and sine components, $A(z)$ and $B(z)$, of the velocity amplitude from the MD simulation as a function of wave propagation distance. The curve fitting was performed for the simulation results obtained with and without the CNT present. The value of the attenuation constant $m_g = 1.05 \times 10^7$ m^{-1} and sound speed $c = 431$ ms^{-1} for the gas were predicted from the waveforms of the velocity components obtained without the CNT present by fitting the curve within the length of the domain $z > 100$ nm, which is equivalent to the CNT region (*Region* 1). Here, the circled (◯) and crossed (×) lines represent velocity components from the MD simulation with and without CNT, respectively. Similarly, the dashed (−−) and solid (−) lines correspond to the fitted data for the velocity components of the simulation with and without CNT, respectively. Different colors of the same line (×, ◯, −, or −−) are used to distinguish between the cosine and sine components, $A(z)$ and $B(z)$, of the velocity amplitude.

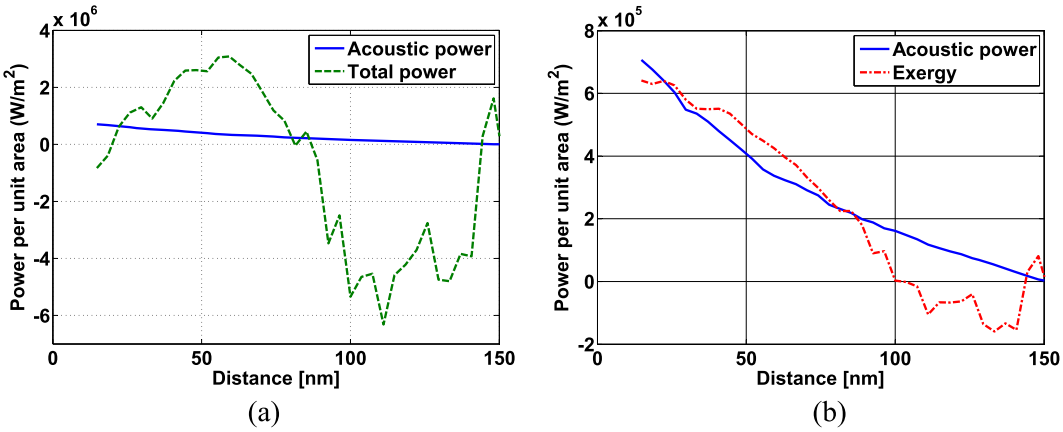

FIG. 9. Comparison of acoustic power [$\dot{E}$ from Eq. (13)] with (a) total power [Eq. (17)] and (b) exergy [combination of Eqs. (19) and (20)] for the simulation containing a CNT.

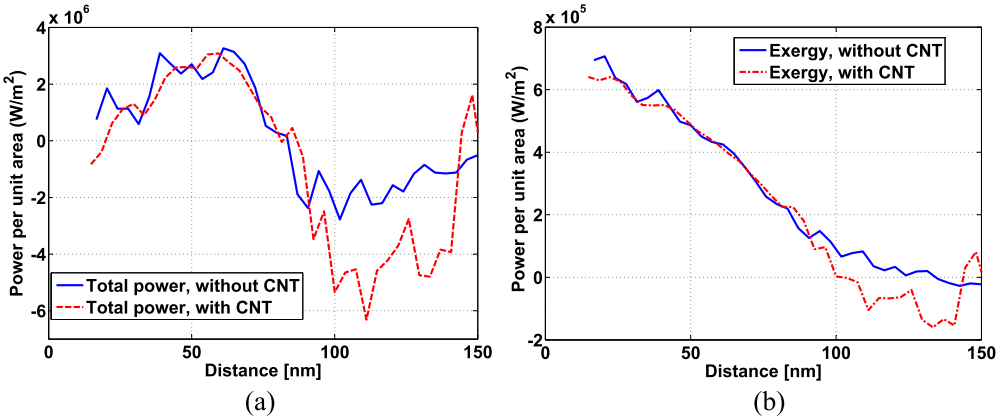

FIG. 10. (a) Total power and (b) exergy in simulations with and without the CNT present.

In the preceding estimates, $m_g = 1.05 \times 10^7$ m^{-1} was obtained from the two-region approach by fitting the velocity profile within $z > 100$ nm (*Region* 1) in the simulation containing gas atoms only. Whereas by considering the original value of $m_g = 0.97 \times 10^7$ m^{-1} obtained from the one-region approach using a single domain of gas atoms without the CNT present (see Appendix A), an estimate of the attenuation coefficient ($m_c + m_g$) for the whole system would give nearly the same value of m_e^{cnt}.

An estimate of the acoustic absorption by the CNT alone can be performed by using the relations in Eqs. (9) and (10). A value of the attenuation by the CNT, $(m_c - m_g) = 1.5 \times 10^6$ m^{-1}, calculated using the curve fitting method, gives an acoustic absorption coefficient of approximately 0.27, indicating 27% absorption by the 50 nm CNT only. This estimate seems reasonable considering that the experimental absorption coefficient obtained for a 3 mm CNT forest (see authors' previous article[10]), which includes millions of CNT per unit area, is 5% ~ 10% for an audible frequency range of 125 Hz–4 kHz. The value estimated here is for a CNT of 50 nm and an acoustic wave of a very high frequency at 1.5 GHz.

V. EFFECTS ON CNT

The transfer of acoustic energy from the gas atoms into the CNT during the wave propagation can also be confirmed by analyzing the atomistic behavior of the CNT. Several aspects of molecular-scale changes to the CNT during wave propagation were analyzed to determine how the attenuation (if any) of the acoustic wave energy is related to the interactions between the CNT and gas atoms. Two primary loss mechanisms[20,36] were anticipated to dominate for sound absorption by the CNT:

- Damping of the wave due to the induced structural vibrations of the material caused by sound pressure and velocity fluctuations within the material. This effect was studied by analyzing the vibrational behavior of the CNT.
- Viscous and thermal losses caused by collisions of the oscillating gas atoms with the CNT atoms and heat conduction due to differences between the thermal conductivity of the wave medium and the CNT. This effect was studied by analyzing the phonon spectrum behavior of the CNT as inelastic collisions between the gas atoms and the CNT would excite phonons along the nanotube and the absorbed energy would be converted to heat by structural damping mechanisms.

A. Vibrational behavior of carbon nanotube

The vibrational behavior of the CNT was analyzed to investigate any significant changes in its structural modes as a result of acoustic wave propagation. To gain further insight

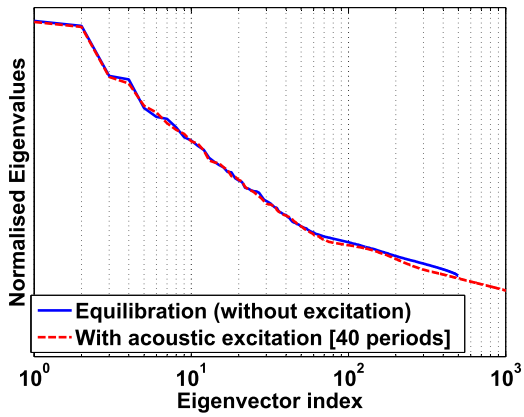

FIG. 11. Deflection modes with and without excitation by the acoustic flow obtained from principal component analysis.

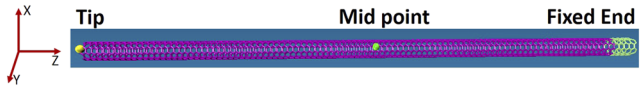

FIG. 12. CNT atom positions used to observe the displacement of the tip and the middle of the CNT.

into the excitation of structural vibrations in the CNT, a principal component analysis (PCA) was performed for the last 40 periods of simulations without (equilibration) and with excitation (acoustic wave), for the atomic trajectory $x_i(t)$, where $i = 1, 2, \ldots, 3N$, where N is the total number of atoms.[31,37] The results of the PCA presented in the scree plot[31] for CNT vibration modes are shown in Fig. 11, which reveals no significant changes in most dominant vibrational modes with or without acoustic excitation.

However, the deflection frequency and energy of the CNT were found to be amplified with acoustic excitation compared with the case without excitation, which can be verified by examining the deflection of an atom at the tip and an atom in the middle of the CNT (as illustrated in Fig. 12). The displacement of the tip and midpoint of the CNT is plotted in Figs. 13 and 14 for simulations with and without acoustic wave excitation. In both cases, Figs. 13 and 14 show that although the amplitude of the deflections does not change significantly with and without acoustic excitation [standard deviation of amplitude (a_x, a_y, a_z) = (1.858 nm, 1.961 nm, 0.102 nm) vs (1.991 nm, 1.696 nm, 0.084 nm) for CNT tip deflections], the deflection frequencies increase significantly with acoustic excitation. The single-sided auto-spectral density of the deflection amplitudes of the midpoint atom in the x-, y-, and z-directions in Fig. 15 reveals the presence of additional peaks at high frequency due to acoustic excitation. Without acoustic excitation, the first three peaks are at frequencies of approximately 1 GHz, 7 GHz, and 40 GHz, which can be attributed to random fluctuations of CNT atoms. With acoustic excitation, an additional peak can be seen at approximately 20 GHz along with the harmonics of this peak at even higher frequencies. Furthermore, the amplitudes of each peak (including those due to thermal fluctuations of CNT atoms) in the auto-spectral densities increased with acoustic excitation. This indicates that a portion of the acoustic energy contributes to amplifying the deflection of the CNT and is also transferred into the normal modes of the CNT that are excited by random fluctuations at equilibrium.

These analyses suggest that the additional energy stored in the CNT atoms during acoustic excitation, due to acoustic energy transfer from the gas atoms into the CNT structure, induces a dramatic increase of the frequency of atom deflections (dx, dy, dz) of the nanotube. This also indicates that the loss of acoustic energy may be attributed to viscous and heat conduction losses due to the collision of gas atoms with the nanotube, thus resulting in the traveling of a phonon down the nanotube. Analysis of the phonon spectrum behavior of the CNT can confirm this hypothesis, as explained in Sec. V B.

It should also be noted here that nonlinear interactions with the nanotubes with respect to the applied forcing may exist, which are beyond the scope of this study and hence are not addressed here. However, investigations of vibrational modes using principal component analysis (PCA) show no significant changes in the eigenvector and eigenvalues with or without acoustic excitation, as shown in Fig. 11. Overall, the structural response resembled a regular linear system and did not show signs of non-linear distortion. Moreover, analysis of the auto-spectral density (ASD) of the deflections of CNT atoms at the tip and in the middle of the CNT, as displayed in Fig. 15, shows that the first two peaks (attributed

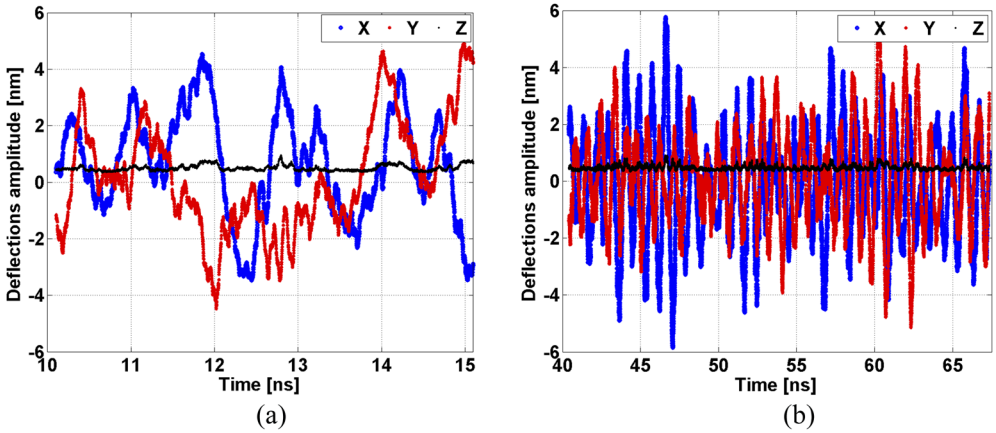

FIG. 13. CNT tip displacement, $(dx, dy, dz) = d(x(t), y(t), z(t)) - d(x(0), y(0), z(0))$ without (a) and with (b) acoustic excitation.

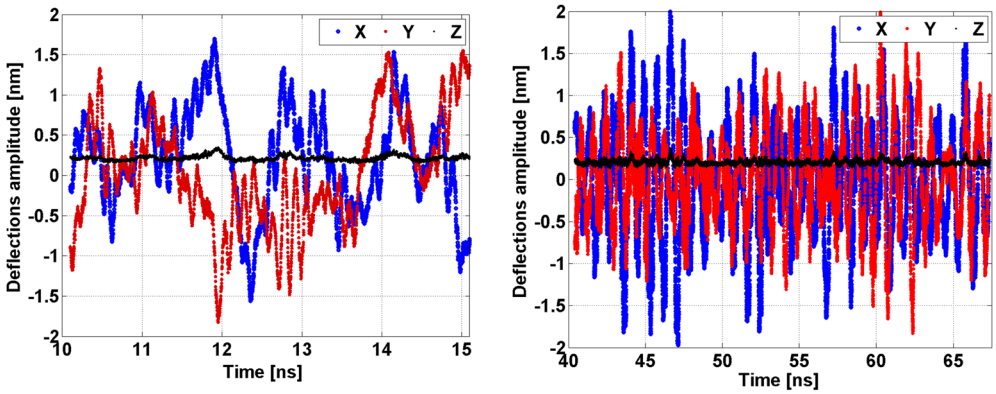

FIG. 14. Displacement of atom in the middle of CNT, $(dx, dy, dz) = d(x(t), y(t), z(t)) - d(x(0), y(0), z(0))$ without (a) and with (b) acoustic excitation.

to the random fluctuations of CNT atoms) are at frequencies of approximately 1 GHz and 7 GHz with or without acoustic excitations and no harmonics of the driving frequency of 1.5 GHz are evident. This analysis indicates that additional resonant interactions due to the additional forcing of the piston at the driving frequency of 1.5 GHz were not significant in the simulation.

B. Phonon spectrum behavior of carbon nanotube

The excitation of phonons by the acoustic wave can be measured by comparing the phonon spectra of the CNT for the cases with and without acoustic excitation. The phonon energy spectrum of the nanotube was calculated from the power spectral density of the velocity fluctuations of carbon atoms in the nanotube as[26]

$$g(f) = \frac{1}{N}\sum_{i}^{N}\left|\int e^{-2\pi i f t}\mathbf{v}_i dt\right|^2, \tag{23}$$

where f is the frequency at which the velocities are sampled from the simulation, $\mathbf{v}_i$ is the velocity of carbon atom i, and N is the total number of atoms in the tube. The velocities were sampled at 133 THz for 66 667 trajectory snapshots

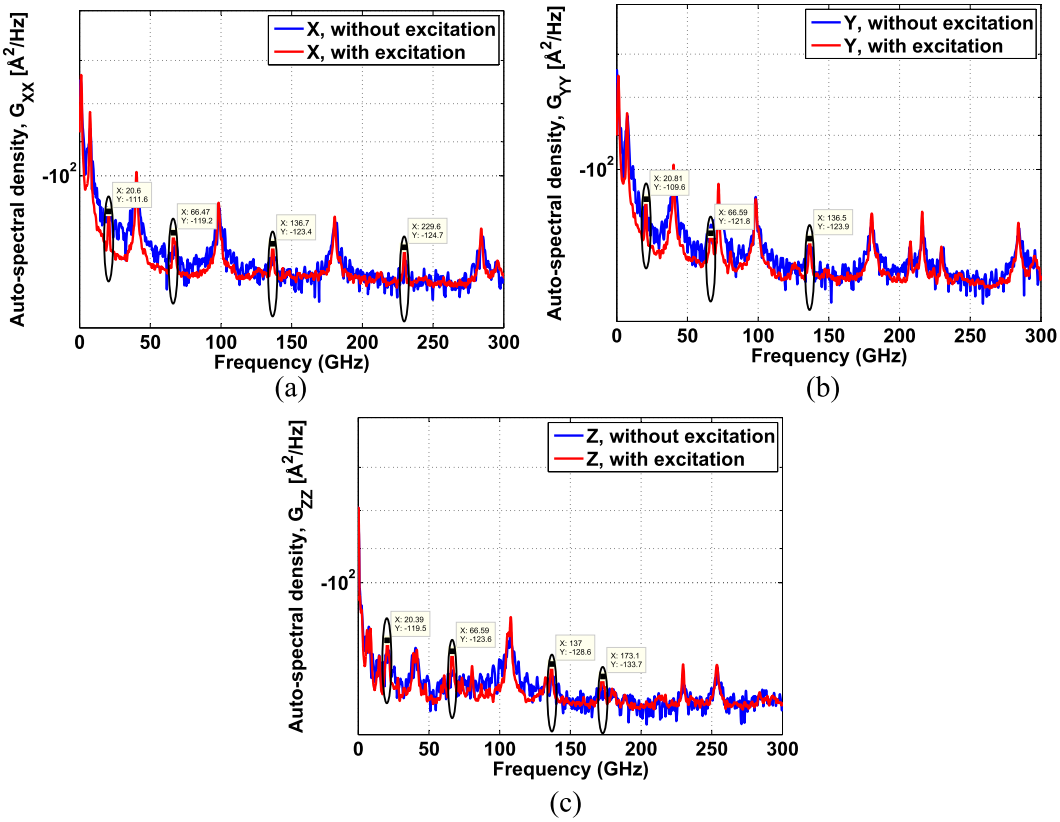

FIG. 15. Single-sided spectrum of the auto-spectral density of the displacement amplitude of the atom in the middle of the CNT, $(dx, dy, dz) = d(x(t), y(t), z(t)) - d(x(0), y(0), z(0))$ with and without excitation. The eclipses in the figures indicate additional peaks of CNT atom deflections. (a) Deflections in the x-direction. (b) Deflections in the y-direction. (c) Deflections in the z-direction.

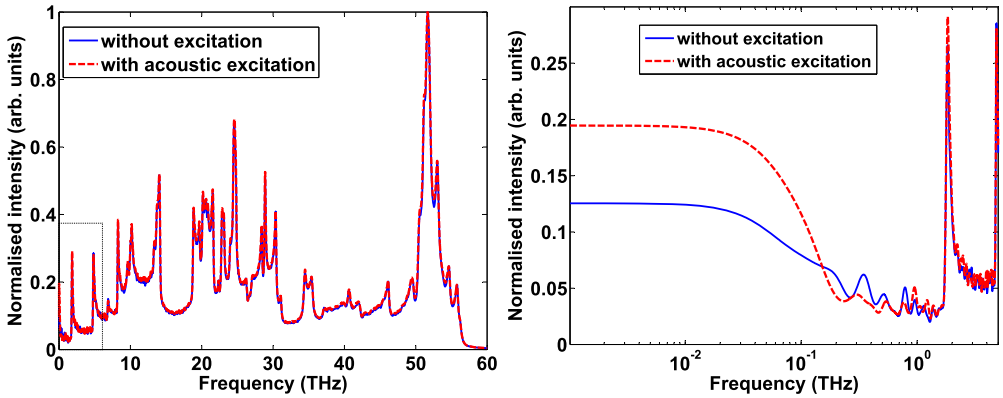

FIG. 16. (a) Phonon energy spectrum of the 50 nm-long SWCNT submerged in an acoustic medium of gaseous argon. The spectra are shown for cases with and without acoustic excitation. A frequency resolution of 0.001 THz was used for the spectrum. (b) Close up of the first 5 THz.

during equilibrium (i.e., without acoustic excitation) and for 89 866 trajectory snapshots during acoustic wave propagation (i.e., with excitation) and ensemble averaged in 2048 sample windows for both cases. The phonon spectrum with acoustic excitations was calculated for only one wave period (between 100 and 101 wave periods) as it was a memory-intensive process to record the velocities of each of the 3990 CNT atoms for a repeated number of wave cycles. Figure 16(a) compares the calculated phonon energy amplitude of the CNT as a function of excitation frequency for the cases with and without acoustic excitation. While no significant differences are visible in the phonon modes over the broadband frequency spectrum of the CNT with and without acoustic excitation, a close up of the phonon spectrum shown in Fig. 16(b) reveals that low-frequency vibrations are excited at frequencies below 1 THz by the acoustic wave, indicating the transfer of energy due to the phonon excitations. Interestingly, significant changes in the phonon energy amplitude occur in the frequency range of 0-100 GHz, which coincides with the earlier observations of the CNT atom deflections at 20 GHz. Excitations of phonons during wave propagation can also be observed at a frequency of 2 THz.

Although the subtle differences in the acoustic properties of the simulated systems with and without the CNT make a detailed analysis of absorption mechanisms challenging, the molecular analyses of the structural vibrational behavior of the CNT, the deflections of the CNT atoms, and the phonon behavior of the CNT confirm that the interactions of the CNT with the acoustic wave have a significant effect on the molecular behavior of the structure, which induce losses of acoustic energy. Possible reasons for not observing more substantial losses induced by the CNT in the current MD setup are as follows:

- Length and positioning of the CNT: The absorption of an absorbent material for any acoustic frequency of interest is greatest when the material is placed at a distance a quarter of the wavelength from a wall, as this is where the particle velocity of the vibrating medium is its highest.[38,39] In the current simulation, the CNT was positioned near the termination wall (reflection wall) and the length of the CNT was L_{CNT} = 50 nm (approximately the distance from the CNT tip to the termination wall), which was smaller than a quarter of a wavelength ($\lambda \approx 290$ nm) of the simulated acoustic frequency. Hence, a CNT either positioned at $\frac{\lambda}{4}$ away from the wall or with a length greater than a quarter of a wavelength of the acoustic frequency would potentially achieve greater acoustic absorption in the CNT.
- Cross-sectional area of the CNT: The diameter of the CNT simulated in this study was d_{CNT} = 0.69 nm and the mean free path of the wave propagation medium (argon gas) was ≈72 nm. Since the simulation was performed for plane-wave propagation with a normal incidence sound source, the wave strikes the cross-sectional area at the tip of the CNT. This means that the CNT would provide a cross-sectional area considerably smaller than a fraction of a mean free path required for a single collision to occur with gas atoms. Hence, interactions between the gas and CNT atoms were infrequent as observed from the atomic trajectory.

Unfortunately, an MD simulation of a much longer or wider CNT than that used in the current work would be computationally prohibitive. Additional MD simulation results of a smaller CNT of 25 nm can be found in the supporting information in Appendix C and demonstrate the variation in acoustic absorption with the variation in the size of the CNT.

VI. SUMMARY

A molecular system was modeled in this study to investigate high-frequency acoustic wave propagation and sound absorption in the presence of a CNT using molecular dynamics (MD) simulations. A standing-wave model, namely, a two-region approach, was developed to express standing-wave equations based on plane-wave theory by separating the wave domain into regions with different attenuation coefficients consisting of the gas atoms only and of the gas atoms and the CNT. These wave equations were used to determine the sound speed and attenuation coefficients for the two regions by performing nonlinear fits to the velocity components obtained from the

MD simulation with and without the CNT present. The attenuation from the simulation results was also estimated in terms of exergy and compared against the standing-wave model. Both estimates gave a good approximation of the attenuation coefficient for the region consisting of the gas and the CNT. Analysis of the simulation results indicated that acoustic absorption by the CNT could be quantified, and the occurrence of absorption was confirmed by the transfer of energy from the gas to the CNT. The low absorption may be attributed to the positioning and the length of the CNT used in these simulations being smaller than a quarter of a wavelength of the propagating acoustic wave and the diameter of the CNT being too small to have frequent collisions with gas molecules. The molecular behavior of the CNT during the acoustic wave propagation was also studied. The frequency of deflections of CNT atoms was found to increase dramatically due to their interactions with the acoustic wave. However, only weak coupling was found between the CNT structure and the propagating acoustic wave as no significant change in the vibrational modes was observed in the CNT structure. In summary, a platform for MD simulations was developed to model and employed to quantify significant acoustic absorption by a nanomaterial. This platform could be extended to investigate loss mechanisms in the audible frequency range and would be beneficial to demonstrate the acoustic behavior of CNT absorbers similar to those studied experimentally.

ACKNOWLEDGMENTS

This research was supported under Australian Research Council's Discovery Projects funding scheme (Project No. DP130102832). The assistance of Mr. Jesse Coombs with the simulations is greatly appreciated. This work was supported by computational resources provided by eResearchSA (https://www.ersa.edu.au/).

APPENDIX A: FORMULATION OF STANDING WAVE EQUATIONS: TWO-REGION APPROACH

In order to perform the analysis using nonlinear curve fitting of velocity components, standing wave equations based on classical acoustic wave theory were formulated for an acoustic domain incorporating a CNT by considering two separate domains between the source and receiver, as illustrated in Fig. 2. As the piston oscillates harmonically at a frequency ω, then the superposition of the incident and reflected waves on each side leads to a standing wave of the form

$$v_c(z,t) = A_1\ \exp[i(\omega t - kz) - m_c z] - B_1\ \exp[i(\omega t + kz) + m_c z], \tag{A1}$$

and

$$v_g(z,t) = A_2\ \exp[i(\omega t - kz) - m_g z] - B_2\ \exp[i(\omega t + kz) + m_g z], \tag{A2}$$

on the right and left sides of the domain, respectively. Subscripts c and g in Eqs. (A1) and (A2) denote the CNT and gaseous region representing the right (*Region* 1) and left (*Region* 2) sides, respectively, of the simulation domain separated at $z = L'$. *Region* 2 is the domain between the source and tip of the CNT which contains only argon atoms, namely, the gas region, and *Region* 1 is for the remainder of the domain which contains both argon and a CNT, namely, the CNT region. The terms A_1, A_2 and B_1, B_2 are the incident and reflected velocity amplitudes, respectively, of the generated standing waves in *Region* 1 and *Region* 2 of the simulation domain. Both A and B can be determined by the boundary conditions at $z = 0$, $z = L$, and $z = L'$. At $z = 0$, the particle velocity of the incident wave would be equal to the velocity variation of the piston or oscillating wall, which can be realized as

$$A_2\ \exp[i\omega t] = v_0 \exp[i\omega t]. \tag{A3}$$

Similarly at the termination wall at $z = L$, the velocity $v_c = 0$, which can be expressed as

$$A_1\ \exp[-(ik + m_c)L] = B_1\ \exp[(ik + m_c)L]. \tag{A4}$$

At the boundary between the regions, the acoustic impedance (as a ratio of pressure and particle velocity) for both regions near to $z = L'$ would be equal, which can be expressed as

$$\frac{A_1 - B_1 \exp[(ik + m_c)2L']}{A_1 + B_1 \exp[(ik + m_c)2L']} = \frac{A_2 - B_2 \exp[(ik + m_g)2L']}{A_2 + B_2 \exp[(ik + m_g)2L']}. \tag{A5}$$

These known boundary conditions can be used to derive a generalized standing wave equation of the developed wave forms in both regions of the simulation domain. By combining Eqs. (A3)–(A5), the generalized form of the standing wave equation can be written as

$$v_{g/c}(z,t) = A_{g/c}(z)\ \sin\omega t + B_{g/c}(z)\ \cos\omega t, \tag{A6}$$

where $A_{g/c}(z)$ and $B_{g/c}(z)$ are the components of the velocity amplitude of the standing wave on each side and can be expressed separately for the CNT (*Region* 1) and the gas regions (*Region* 2), as written in Eqs. (2)–(5).

The non-linear fitting of these equations to the components of the velocity amplitudes for a theoretical standing wave

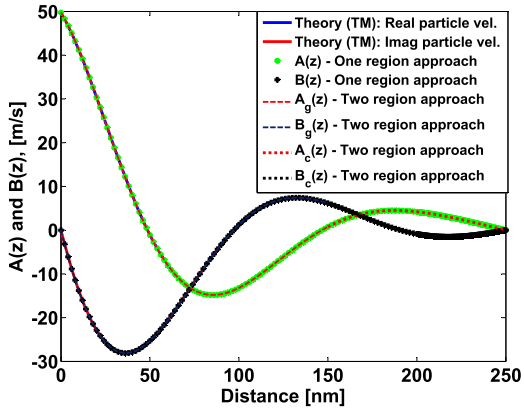

FIG. 17. Comparison between one- and two-region approaches for non-linear fitting of the wave equations to the components of the velocity amplitude for a theoretical standing wave formulated using a transmission matrix for an acoustic wave of frequency $f \approx 2.5$ GHz ($R = 0.5$). The length of the domain $z < 150$ nm represents the gas region (*Region* 2), and the domain length $z > 150$ nm corresponds to the CNT region (*Region* 1). The waveforms fit perfectly to the velocity components for both approaches and predict the same value of the sound speed and attenuation coefficient as the value used to formulate the standing wave.

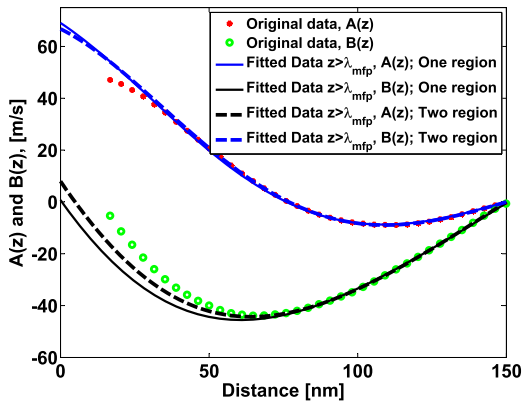

FIG. 18. Comparison between one- and two-region approaches for non-linear fitting of the wave equations to the components of the velocity amplitude from the simulation results for a case without the CNT (with the solid argon wall as an acoustic source) for an acoustic wave of frequency $f \approx 1.5$ GHz ($R = 1$). The length of the domain $z < \lambda_{\text{mfp}}$ represents the gas region (*Region* 2), and the domain length $z > \lambda_{\text{mfp}}$ corresponds to the CNT region (*Region* 1). Predicted values: the one-region approach-c = 446 ms^{-1}, $m = 0.967 \times 10^7$ m^{-1}; the two-region approach-c = 429 ms^{-1}, $m = 0.952 \times 10^7$ m^{-1}.

can be used to compare the acoustic variables obtained from the one-region [Eqs. (6) and (7)] and two-region [Eqs. (2)–(5)] approaches. The transmission matrix method[15,24] was used to formulate a profile of the velocity components of a theoretical standing wave using acoustic variables such as the piston velocity amplitude $v_0 = 49.39$ ms^{-1}, sound speed $c = 500$ ms^{-1}, attenuation coefficient $m = 1.34 \times 10^7$ m^{-1}, and frequency $f \approx 2.5$ GHz. Figure 17 shows the fitting of the wave forms to the theoretical standing wave using both approaches. The predicted values of the acoustic variables such as the sound speed and attenuation were found to be the same as the values used to formulate the theoretical standing wave. This confirms that the two-region approach can predict the same value of the attenuation coefficients for two adjacent regions if both have the same medium.

The two-region approach was also used to predict the sound speed (c) and attenuation coefficient (m) from the simulation results of the velocity components for an acoustic domain without the CNT present for a wave of frequency $f \approx 1.5$ GHz. A comparison of the two approaches (one and two regions) for the non-linear fits of the waveforms is shown in Fig. 18. The predicted values of c and m are 446 ms^{-1} and 0.967×10^7 m^{-1} and 429 ms^{-1} and 0.952×10^7 m^{-1} by using the one- and two-region approaches, respectively. The difference in the attenuation coefficient is due to the variation in the sound speed between the two approaches. However, if a constant value of c were used for the prediction in the two-region approach, then both attenuation coefficients would have been the same. It can be seen from Fig. 18 that both approaches give a good fit to the waveforms for constant values of the sound speed and attenuation coefficient within the data fitting region at distances further than one mean free path ($z > \lambda_{\text{mfp}} = 7.28 \times 10^{-8}$ m).

APPENDIX B: STEADY STATE CONDITION DURING WAVE PROPAGATION

The variation of the temperature of both the gas and the CNT, of the gas pressure during the wave propagation, is shown in Figs. 19(a) and 19(b), respectively. It can be seen that both the gas and the CNT reached a steady mean temperature after 40 periods. The increase in the average temperature and pressure of the gas, which reached 284 K and 1.09 bars (≈1 atm), was within 5% of the equilibrium temperature and pressure in the absence of wave propagation (273 K and 1 atm, respectively), which confirms that the change of sound speed would be less than 2.5% since the sound speed varies as $\sqrt{T}$.[21]

The energy balance of the system was investigated to ensure consistency between the energy input, the energy stored, and the energy dissipated. The acoustic energy input into the system is equal to the work done by the piston, which can be calculated from the measured normal force on the gas and the oscillating displacement of the piston. Figure 20 shows a complete history of the energy due to the work done by the piston and the energy extracted by the thermostat as a function of the oscillation period of the wave cycle during the acoustic wave propagation. A linear fit of these two curves of almost identical slopes gives the work done by the piston and the energy extracted by the thermostat as approximately 509 kcal/mol and 507 kcal/mol per period, respectively.

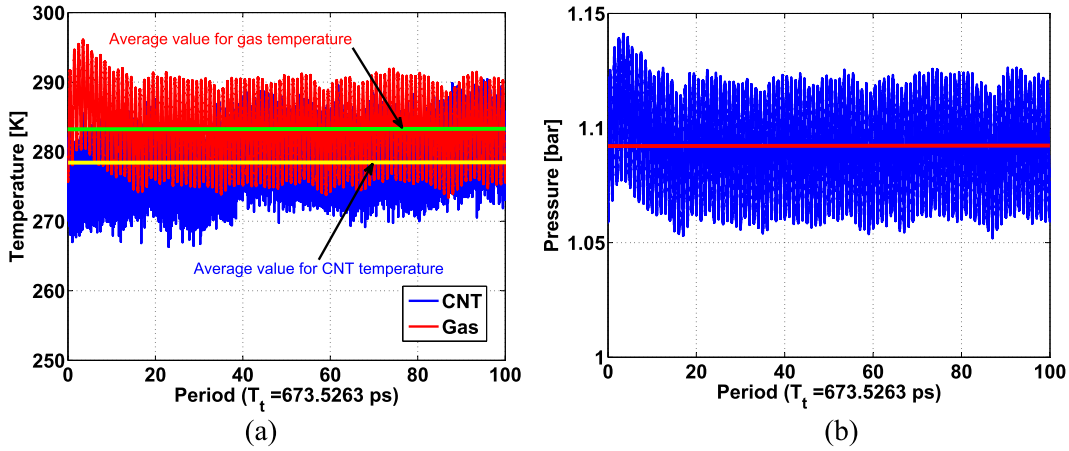

FIG. 19. Variation (a) temperature of the gas and the CNT and (b) pressure of the gas for a simulation of acoustic wave propagation with the CNT present in the acoustic domain.

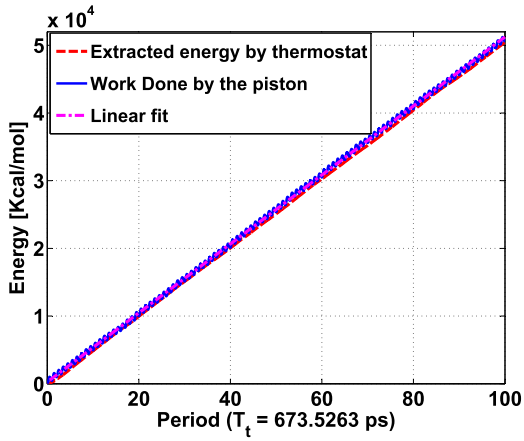

FIG. 20. Comparison of the work done by the piston and the energy extracted by the thermostat as a function of the oscillation period of the wave cycle for a simulation domain incorporating a CNT for acoustic excitation at frequency $f \approx 1.5$ GHz ($R = 1$).

This indicates that an approximate energy balance per acoustic wave period is maintained between the energy input by oscillations of the piston and the extraction of energy from the system by the thermostat. The small discrepancy can be attributed to the linear fitting of the curve for all wave periods, which includes the transition periods between the steady state condition and equilibration.

APPENDIX C: COMPARISON WITH MD SIMULATION RESULTS OF A 25 nm-LONG CNT

Due to the limited availability of computational resources, simulations were restricted to a relatively short and narrow CNT 50 nm in length and 0.69 nm in diameter in a small acoustic domain. An MD simulation of a significantly longer or wider CNT than that used in the current work would be computationally prohibitive using the available computational resources. Research is currently being carried out in our group to speed up the simulations.[40]

To demonstrate the variation in acoustic absorption with that of the CNT length, we have instead compared simulation results of the 50 nm-long CNT for an acoustic frequency of 1.5 GHz with that those for a shorter 25 nm-long CNT of the same diameter for wave propagation at a higher acoustic frequency of 2.57 GHz. Figure 21 compares the acoustic power and exergy for the two cases. The significantly different behavior of the acoustic power and exergy for the different nanotubes indicates differences in the acoustic wave energy in the two systems. The differences between the exergy and acoustic power for wave propagation at 2.57 GHz for the simulation of the 25 nm CNT are not statistically significant in the region where the CNT is situated ($z > 125$ nm) as the acoustic energy in that region is not strong enough to have a considerable interaction of the acoustic wave with the CNT. On the other hand, the differences between the exergy and acoustic power become significant and more pronounced with the longer 50 nm CNT at a lower frequency of 1.5 GHz in the region where the CNT is situated ($z > 100$ nm), indicating an increase in wave attenuation due to higher absorption by the longer CNT and higher acoustic energy.

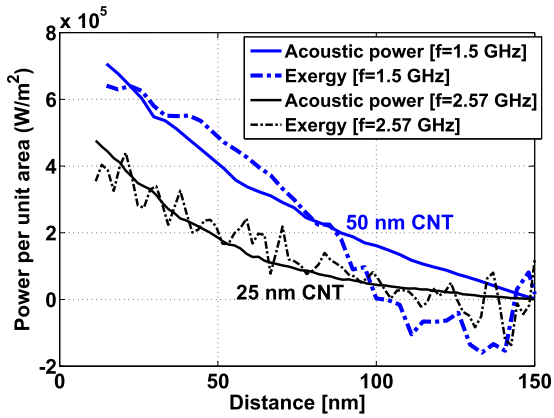

FIG. 21. Comparison of acoustic power and exergy between the simulations of acoustic frequencies of $f \approx 1.5$ GHz and 2.57 GHz with 50 nm and 25 nm CNTs, respectively.

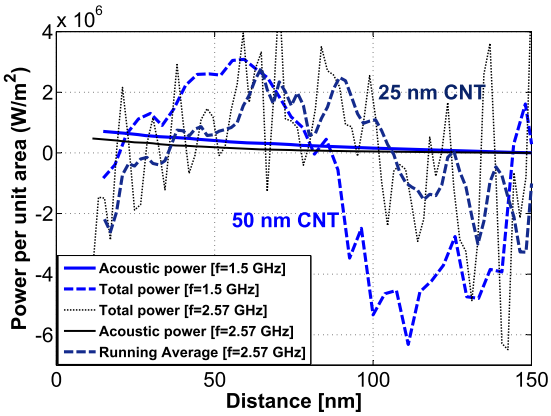

FIG. 22. Comparison of acoustic power and total power between the simulations of acoustic frequencies of $f \approx 1.5$ GHz and 2.57 GHz with 50 nm and 25 nm CNTs, respectively. Simulation results of 25 nm CNT with acoustic frequency of 2.57 GHz are noisy as the wave gets attenuated (much quickly compared to the lower frequency of 1.5 GHz) as it moves away from the sound source.

A similar difference between the acoustic power and total power can be seen in Fig. 22, which compares the acoustic power and total power for the two cases. The differences are the largest near the CNT region ($z > 125$ nm for the 25 nm CNT and $z > 100$ nm for the 50 nm CNT) of the domain and are more pronounced for the longer CNT. These variations in the computational results between two cases with two different lengths of CNTs demonstrate that a CNT longer than one quarter of a wavelength would achieve greater absorption.

[1] P. Ajayan, A. Carrillo, N. Chakrapani, R. S. Kane, and B. Wei, "Carbon nanotube foam and method of making and using thereof," U.S. patent Application No. 11/005474, Patent No. USOO7473411 B2 Rensselaer Polytechnic Institute (January 6, 2009).
[2] W. Cho, M. Schulz, and V. Shanov, "Growth and characterization of vertically aligned centimeter long CNT arrays," Carbon **72**, 264–273 (2014).
[3] W. Cho, M. Schulz, and V. Shanov, "Growth termination mechanism of vertically aligned centimeter long carbon nanotube arrays," Carbon **69**, 609–620 (2014).
[4] M. F. De Volder, S. H. Tawfick, R. H. Baughman, and A. J. Hart, "Carbon nanotubes: Present and future commercial applications," Science **339**, 535–539 (2013).
[5] Y. J. Qian, D. Y. Kong, Y. Liu, S. M. Liu, Z. B. Li, D. S. Shao, and S. M. Sun, "Improvement of sound absorption characteristics under low frequency for micro-perforated panel absorbers using super-aligned carbon nanotube arrays," Appl. Acoust. **82**, 23–27 (2014).

[6]J. Cherng, "Smart acoustic materials for automotive applications," Technical Report for Project No. 2005/3, Henry W Patton Center for Engineering Education and Practice, The University of Michigan-Dearnborn, 2006.
[7]M. Bandarian, A. Shojaei, and A. M. Rashidi, "Thermal, mechanical and acoustic damping properties of flexible open-cell polyurethane/multi-walled carbon nanotube foams: Effect of surface functionality of nanotubes," Polym. Int. **60**, 475–482 (2011).
[8]R. Verdejo, R. Stämpfli, M. Alvarez-Lainez, S. Mourad, M. Rodriguez-Perez, P. Brühwiler, and M. Shaffer, "Enhanced acoustic damping in flexible polyurethane foams filled with carbon nanotubes," Compos. Sci. Technol. **69**, 1564–1569 (2009).
[9]S. Basirjafari, R. Malekfar, and S. E. Khadem, "Low loading of carbon nanotubes to enhance acoustical properties of poly(ether)urethane foams," J. Appl. Phys. **112**, 104312 (2012).
[10]M. Ayub, A. C. Zander, C. Q. Howard, B. S. Cazzolato, V. N. Shanov, N. T. Alvarez, and D. M. Huang, "Acoustic absorption behavior of carbon nanotube arrays," in *43rd International Congress on Noise Control Engineering (Inter-Noise 2014)*, The Australian Acoustical Society (Melbourne, Australia, 2014), Vol. 249, pp. 929–938.
[11]M. Ayub, A. C. Zander, C. Q. Howard, B. S. Cazzolato, D. M. Huang, V. N. Shanov, and N. T. Alvarez, "Acoustic absorption behaviour of a tall carbon nanotube forest," in *Proceedings of Acoustics 2016* (Brisbane, Australia, 2016), pp. 1–10.
[12]M. Ayub, A. Zander, C. Howard, B. Cazzolato, D. Huang, V. Shanov, and N. Alvarez, "Normal incidence acoustic absorption characteristics of a carbon nanotube forest," Appl. Acoust. **127**, 223–229 (2017).
[13]M. Ayub, A. C. Zander, C. Q. Howard, and B. S. Cazzolato, "A review of acoustic absorption mechanisms of nanoscopic fibres," in *Proceedings of Acoustics 2011* (Gold Coast, Australia, 2011), pp. 77–84.
[14]M. Ayub, A. C. Zander, C. Q. Howard, B. S. Cazzolato, and D. M. Huang, "A review of MD simulations of acoustic absorption mechanisms at the nanoscale," in *Proceedings of Acoustics 2013* (Victor Harbor, Australia, 2013), pp. 19–26.
[15]M. Ayub, A. C. Zander, C. Q. Howard, D. M. Huang, and B. S. Cazzolato, "Molecular dynamics simulations of sound wave propagation in a gas and thermo-acoustic effects on a carbon nanotube," in *International Conference on Theoretical and. Computational Acoustics (ICTCA), Special Issue* [J. Comput. Acoust. **23**, 1540012-1–1540012-18 (2015)].
[16]F. Fahy, *Foundations of Engineering Acoustics* (Elsevier Academic Press, London, UK, 2005), Chap. 7.
[17]U. Ingard, *Noise Reduction Analysis* (Jones and Bartlett Publishers; Science Press, LLC, USA, 2009), Chap. 2.
[18]J. Allard and N. Atalla, *Propagation of Sound in Porous Media: Modelling Sound Absorbing Materials*, 2nd ed. (John Wiley & Sons, Ltd., UK, 2009), Chap. 4, Secs. 4.2-4.3, pp. 45–53.
[19]C. Q. Howard and B. S. Cazzolato, *Acoustic Analysis Using Matlab and Ansys* (CRC Press, 2014).
[20]L. Kinsler, A. Frey, A. Coppens, and J. Sanders, *Fundamentals of Acoustics*, 4th ed. (John Wiley & Sons, Inc., New York, 2000), Chap. 8, Secs. 8.1-8.5, pp. 210–218.
[21]N. G. Hadjiconstantinou and A. L. Garcia, "Molecular simulations of sound wave propagation in simple gases," Phys. Fluids **13**, 1040–1046 (2001).
[22]G. W. Swift, *Thermoacoustics: A Unifying Perspective for Some Engines and Refrigerators* (Acoustical Society of America, New York, 2002), Chap. 6, Secs. 6.1-6.2, pp. 147–158.
[23]M. Ayub, A. C. Zander, D. M. Huang, C. Q. Howard, and B. S. Cazzolato, "Molecular dynamics simulations of classical sound absorption in a monatomic gas," J. Sound Vib. **421**, 319–333 (2018).
[24]L. L. Beranek and I. L. Ver, *Noise and Vibration Control Engineering: Principles and Applications* (John Wiley and Sons, New York, USA, 1992), p. 377.
[25]D. W. Brenner, O. A. Shenderova, J. A. Harrison, S. J. Stuart, B. Ni, and S. B. Sinnott, "A second-generation reactive empirical bond order (REBO) potential energy expression for hydrocarbons," J. Phys.: Condens. Matter **14**, 783 (2002).
[26]C. F. Carlborg, J. Shiomi, and S. Maruyama, "Thermal boundary resistance between single-walled carbon nanotubes and surrounding matrices," Phys. Rev. B **78**, 205406 (2008).
[27]S. Maruyama, "A molecular dynamics simulation of heat conduction of a finite length single-walled carbon nanotube," Microscale Thermophys. Eng. **7**, 41–50 (2003).
[28]S. Maruyama, "Molecular dynamics methods in microscale heat transfer," in *Heat Transfer and Fluid Flow in Microchannels* (Begell House, Inc., 2002), Chap. 2.13.
[29]J. Shiomi and S. Maruyama, "Non-Fourier heat conduction in a single-walled carbon nanotube: Classical molecular dynamics simulations," Phys. Rev. B **73**, 205420-1–205420-7 (2006).
[30]J. D. Weeks, D. Chandler, and H. C. Andersen, "Role of repulsive forces in determining the equilibrium structure of simple liquids," J. Chem. Phys. **54**, 5237–5247 (1971).
[31]C. Chen, M. Ma, K. Jin, J. Z. Liu, L. Shen, Q. Zheng, and Z. Xu, "Nanoscale fluid-structure interaction: Flow resistance and energy transfer between water and carbon nanotubes," Phys. Rev. E **84**, 046314 (2011).
[32]L. Kinsler, A. Frey, A. Coppens, and J. Sanders, *Fundamentals of Acoustics*, 4th ed. (John Wiley & Sons, Inc., New York, 2000).
[33]F. Jacobsen, "Active and reactive, coherent and incoherent sound fields," J. Sound Vib. **130**, 493–507 (1989).
[34]E. Kuipers, "Measuring sound absorption using local field assumptions," Ph.D. thesis, University of Twente, Enschede, The Netherlands, 2013.
[35]G. W. Swift, *Thermoacoustics: A Unifying Perspective for Some Engines and Refrigerators* (Acoustical Society of America, New York, 2002), Chap. 5, Sec. 5.2, pp. 128–134.
[36]A. F. Seybert, "Sound absorption by porous materials," Lecture Sildes ME 599/699, Department of Mechanical Engineering, University of Kentucky, 2002.
[37]P. M. Shenai, Z. Xu, and Y. Zhao, "Applications of principal component analysis (PCA) in materials science," in *Principal Component Analysis–Engineering Applications* (InTech, 2012), Chap. 2.
[38]T. J. Cox and P. D. Antonio, *Acoustic Absorbers and Diffusers–Theory, Design and Application*, 2nd ed. (Taylor and Francis, London and New York, 2009).
[39]P. R. Newell, *Recording Studio Design* (Focal Press, UK, 2003).
[40]H. A. Bennett, A. C. Zander, B. S. Cazzolato, and D. M. Huang, "Speedup techniques for molecular dynamics simulations of the interaction of acoustic waves and nanomaterials," in *The 21st International Congress on Modelling and Simualtion (MODSIM2015)* (Queensland, Australia, 2015).